31 August 2023
magnus.thoegersen@cern.ch

# System performance monitoring of the CLICdp Timepix3 test beam telescope

Author: Magnus Thøgersen
Supervisors: Peter Svihra & Justus Braach

Keywords: Beam Telescope, Monitoring, Raspberri Pi, MIKROE, Adafruit, Python, Semiconductor Detectors, High Energy, Particle Physics

Summary

This project centers around the EP PIXEL CLICdp Timepix3 Beam Telescope and its ongoing improvements, specifically regarding alignment shift and monitoring. In order to improve the efficiency of data taking and general reliability metrics are logged during a running measurement. This includes measurement progress, DAQ data rates, storage volume and position measurements of the devices in the setup. Furthermore a recently added compressor cart was installed introducing a low volume dry air flow, improving the air-circulation and providing a consistent and enhanced heat dissipation for the detector planes of the telescope. With the cart a series of small sensors monitoring the air and its flow through the telescope. With these new sensors and through analysis of test beam measurement data, the shifts in telescope plane alignment could be put in relation to observables of the telescope environment, by comparing detector plane displacement data with changes in temperature. It was found that there is a correlation between the two with shifts along the cartesian axes in a range of 2 µm and also angularly within a range of 1 degree.

# Contents

# 1 Introduction

To fulfil the demanding requirements for future vertex- and tracking-detectors in High Energy Physics, silicon pixel detector technologies are continuously being developed and optimized. However, before they can be considered for use in actual experiments, their performance must be evaluated. Within the CERN EP Department a strategic R&D programme with 11 work packages (WP) was defined, that is, among other technologies, also advancing silicon pixel detector technologies. In this endeavor particle beam tests are of central importance, and specifically beam telescopes serve as reference tracking systems that provide spatial as well as temporal information about the particle tracks. The CLICdp Timepix3 beam telescope, which started its operation as part of the CLIC (Compact Linear COllider) vertex tracker programme, is now continuing on as a reference particle tracking system for general pixel detector R&D in CERN's EP R&D. In order to improve the data taking efficiency and the reliability as well as prepare the telescope for the requirements of future pixel detector technology demonstrator chips the EP-DT-TP section seeks to improve the telescope system continuously.

One so far unmonitored aspect of the system is a shift in position of the telescopes' detector planes over time which have to be realigned in software every day of data taking. A correlation of the shifts with periodic changes in environmental observables of the telescope setup such as temperature or humidity is to be investigated. In this project report the CLICdp telescope will be discussed in Section 2.1 followed up by focusing on the software alignment process of the detector planes in Section 3.1. Furthermore the implementation of new equipment, designed to improve the setup as well as to monitor environmental observables of the telescope, which can be seen in Section 3.

# 2 Experimental Setup & Data Processing

In this section the EP PIXEL CLICdp Timepix3 Beam Telescope, its components as well as the Corryvreckan reconstruction framework will be introduced.

## 2.1 Telescope

The EP PIXEL CLICdp Timepix3 Beam Telescope, installed at the CERN SPS North Area test-beam facility, is used for the characterization of various silicon detector technologies. The central part of the telescope consists of six Timepix3 detector planes, which are tilted in order to optimize their spatial resolution, as well as three scintillator planes attached to photo-multiplier tubes (PMTs) and a microchannel plate detector (MCP). The setup can be seen in Figure 1.

### 2.1.1 Timepix3 detector assemblies

The Timepix3[1] detector assembly is made from a general-purpose Timepix3 readout ASIC (Custom Application Specific Integrated Circuits) designed by the Medipix Collaboration. It has a matrix size of 256 × 256 pixels and a pixel pitch of 55 µm × 55 µm, spacing each pixel center 55 µm away from its closest neighbour in the grid. The ASIC is suitable for readout

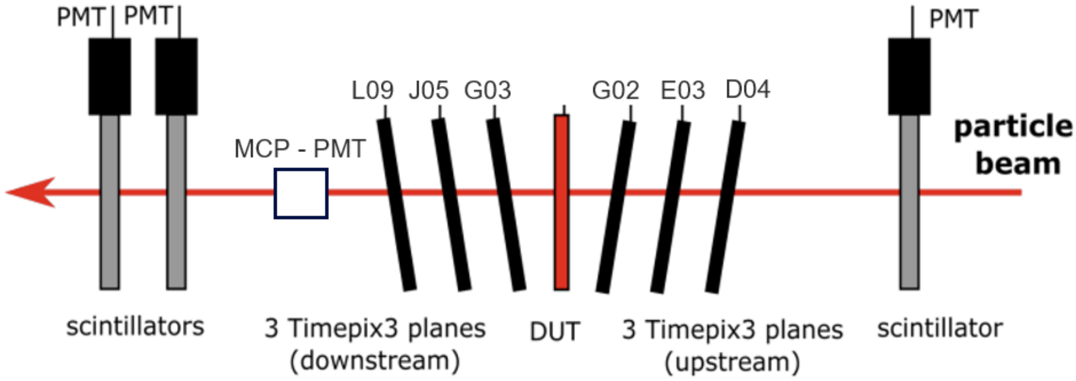


Figure 1: CLICdp Timepix3 telescope test-beam setup

of both semiconductor detectors as well as gas-filled detectors. In the case of the telescope application, the Timepix3 ASICs are each bump bonded to to a 300 µm thick p-on-n planar Si-sensor[1] (see Section 2.1.2 for explanation on Si-sensors).


Figure 2: Pictures of the the chipboard for the Timepix3 detector planes. left) back, right) front

Compared to its predecessors the ASIC has more functionality, better time resolution and generally more advanced architecture. And although its successor, the Timepix4, which was introduced 2019, would be considered superior in a number of ways (see section Appendix A for table comparing the different models), the Timepix3 still remains a considerable choice due to its reliability, availability and the readily available documentation of multiple applications in similar cases[2]. To read out the measured data from each telescope plane, SPIDR (Speedy Pixel Detector Readout) FPGA (Field Programmable Gate Array) boards are used, a setup designed as a general readout platform for pixelated readout ASICs, such as Timepix3[3]. The detector assemblies connect to the SPIDR boards on top of the telescope enclosure through coaxial ribbon cables and further on through optical links to a measurement server. Here the data is then stored and can be accessed for analysis[4].

### 2.1.2 Silicon sensors

Most Si-sensors used presently in vertex tracker applications are of the so-called planar structure type, which is also the type used in the telescope. The silicon wafer will either be negatively- or positively-doped, meaning that impurities will be introduced to modify the conductivity. In single-sided detectors, one side of the wafer is structured with implantation of the opposite type. The sensors used in the telescope planes are of the p-on-n type. By applying an external reverse bias voltage to the sensor a depletion zone is created, which means that all the charge carriers that would normally be present in the material are forced away by the applied electric field. This volume thereby becomes sensitive to the charge generated by ionizing particles similarly to the gap in a capacitor. When struck by an ionizing particle within the Silicon bulk, the charge carriers (electrons and holes) are created in the sensitive silicon layer and then separated by their polarity following the electric field gradient. This drift of the newly created charge carriers provides an electrical signal that is registered by electrodes and then can be read out.[5]

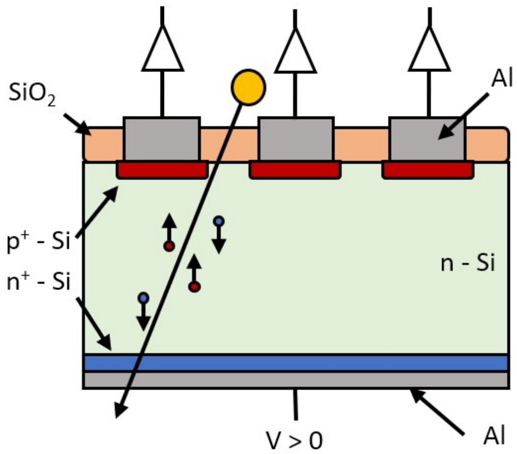


Figure 3: Illustration of the workings of a Si-sensor reacting to a charged particle

### 2.1.3 Time reference and coincidence

The scintillator paddles and the attached PMTs provide time reference in the order of hundreds of picoseconds and are used as a coincidence selection on the particles passing through the telescope setup. The beam particles are absorbed by the scintillator material, leading to the creation of primary electron-hole pairs. These pairs generate secondary pairs that move through the material before they undergo radiative-recombination and produce photons. The photons then pass to the PMT and its photocathode, creating a so-called primary electron. This electron moves towards the focusing electrode and gets passed along to the electron multiplier consisting of a series of dynodes that create new electrons through the process of secondary emission. At the end these electrons are read out by the anode as an electrical signal. The simultaneous arrival of signals from all three scintillators is evaluated for temporal coincidence by a NIM-unit and gives information of whether a particle has crossed the active areas of all three scintillators. This information can be used for tuning the acceptance of the telescope normal to the beam and can on top of that be used as time stamping information for track reconstruction. With the increasing temporal measurement precision of state-of-the-art pixelated silicon detector protoypes, a 10ps precission time reference is needed for the telescope in order to accurately be able to characterize demonstrator devices with time measurement precision capabilities of close to 100ps. Just before the start of this project a Micro Channel Plate Photomultiplier Tube (MCP-PMT) of the R3809U series from Hamamatsu[6] was installed, enabling the telescope to cover this very "fast" regime of temporal measurements. An MCP functions in a similar way to a PMT. It is made from a resistive material filled with a regular array of tiny tubes (microchannels). By applying a strong electric field across the MCP, the channels start functioning as continuous-dynode electron multipliers. So when hit by a charged particle, an electrical signal is produced just as for the PMT but with much better precision.

## 2.2 Corryvreckan

### 2.2.1 Setup

The Corryvreckan reconstruction framework is a software tool that allows the user to reconstruct the particle tracks from the information measured by a set of detector planes, which can be used as reference information in comparison with the data measured by a device under test (DUT). It allows one to align the measurements to a high precision and then select tracks that also crossed the DUT. The goal of this is to compare the signals recorded by the DUT in time and space to the reconstructed and selected particle tracks, crossing the DUT with a slightly different location in space ad time, depending on the precision of the device under test.

### 2.2.2 Alignment

An analysis with Corryvreckan requires a geometry file defining which detectors are present in the setup as well as their position and rotation in relation to a reference, which in the case of the telescope was the last of the upstream Timepix3 planes (third from the right in Figure 1), named W0013_G02. The z-coordinate of the detectors described in the geometry file, however, is a fixed parameter within Corryvreckan, as the alignment algorithms are not sensitive to it. Therefore this information is based on manual, external measurements done by an operator. For the analysis a configuration file is needed, containing the different operations in the form of modules that are to be performed on the data from the detectors defined in the geometry file.

To align the telescope planes two processes had to be performed. In the first prealignment the configuration file is loaded with a geometry file as well as a file directory leading to the data of a specific run. These are compared and used to create a root file containing the track data acquired by the planes in the form of plots, as well as an update to the geometry file. By accessing the file through the ROOT T-browser, one is presented with a number of folders relating to the modules of the configuration file. For prealignment the folder named Correlations is accessed, and through subfolders relating to the different telescope planes, the different correlation plots are accesible. Specificaly looking at the correlation in X and Y, the difference of the reference track positions and the hit positions taken from the detector in questions is seen as a sharp peak. If the peak offset from 0 the reference information from the telescope tracks suggests a different hit position than the detector in question, asking for the geometry file to be changed in order to shift the peak towards 0. This can be seen in Figure 4

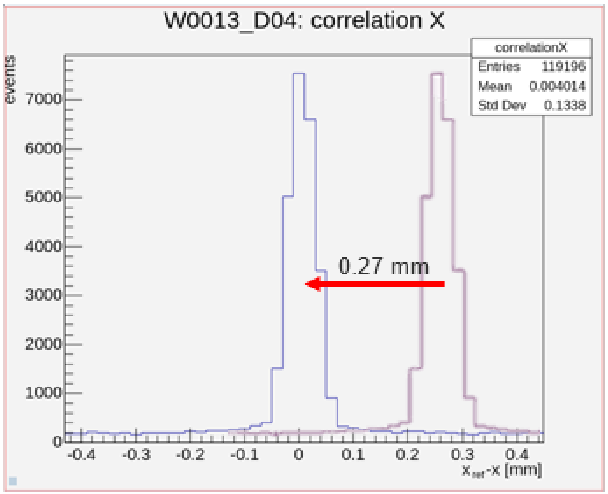


Figure 4: Correlation plot for X coordinate of W0013_D04 illustrating a shifting of a peak before prealignment (right) to after prealignment (left)

Once this is done for all the planes, with exception of the reference plane, the final alignment could take place. Here the [Tracking4D] module was utilized as well as the [AlignmentTrackChi2] module. The [Tracking4D] module creates tracks based on hits registered in planes as long as it is provided with specifications on minimum number of hits, a track model and a spatial as well as temporal cut. It can also be specified if the DUT should be excluded or not, which was chosen for all alignments performed as part of this project. Using the tracking from the [Tracking4D] module, the [AlignmentTrackChi2] module then tries to minimize the $\chi^2$-values for the previously formed track fits. The alignment process the has to be repeated by progressively lowering the spatial cut until reaching pixel pitch (55 µm × 55 µm).

Repeating these processes for a series of runs updates the geometry file for each run and thereby provides a sequence of translational and rotational displacements for each detector plane. This information finally illustrates how the planes shift over time (See section 3.2 for further explanation). Each alignment takes about 20 minutes, and depending on how much work is needed for the manual prealignment, the total time spent on alignment of a single run reaches 30 minutes. The alignment of a multitude of runs thereby ends up as a time-consuming task, and therefore it would make sense to get a better understanding of how alignments change.

# 3 Ongoing improvements

## 3.1 Mechanical alignment

The first upgrade of the telescope setup that was undertaken as part of this project was a characterization of the stability of mechanical alignment over time. In preparation for the 2023 SPS North Area test beam season two-level stacks of rotation (top) and linear stages (bottom) were added to the two posts that support the up- and downstream telescope arms. The now possible translation along the x axis can be used to shift an entire arm in x as well as apply a slight rotation by moving the two linear stages in opposite directions.
With this the mechanical alignment of the telescope arms with respect to each other already was improved to a remaining offset of 0.1 mm. The before-mentioned scintillator planes similarly received an upgrade in adjustment by the addition of linear stages along the x- and y- axis. The latter is allowing the telescope operator to deliberately place them in order to maximize or specifically constrain the track acceptance of the telescope within 50 µm accuracy in the vertical plane. Thereby the telescope could be set up more precisely in preparation for a measurement campaign, improving the overall alignment.

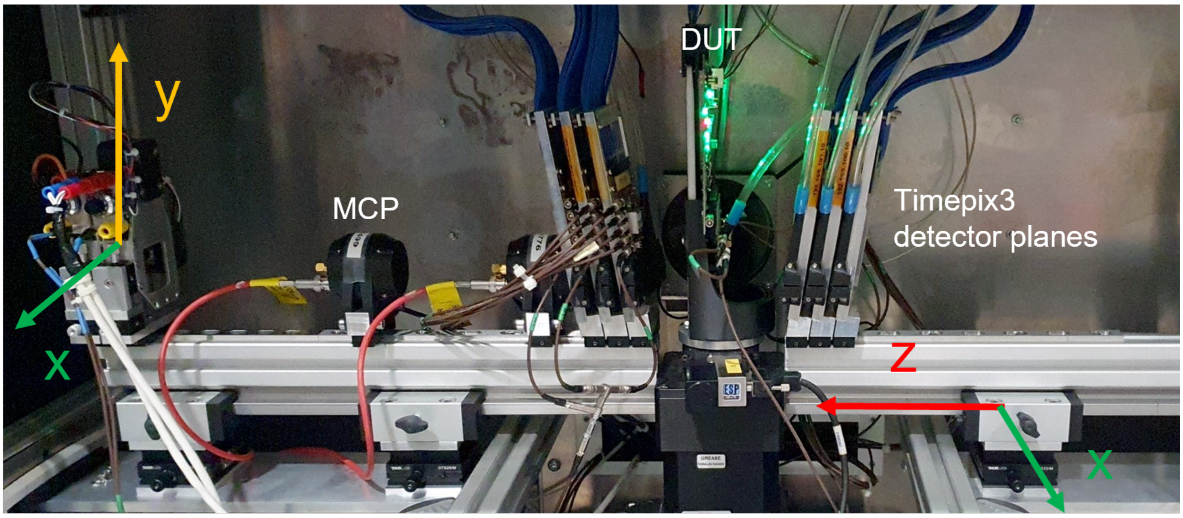


Figure 5: Pictures the detector setup

A higher-precision alignment of the telescope planes is achieved by using the particle track information in software track reconstruction algorithms. At this stage the final alignment of each individual detector plane was accomplished using the previously mentioned Corryvreckan reconstruction framework.

## 3.2 Verification of alignment stability

In this section a selection of plots created based on alignment data gathered from the geometry files of various runs using the Corryvreckan reconstruction framework will be shown and discussed.

### 3.2.1 Alignment verification

To validate the alignment and deem whether the plots of alignment shift are accurate, one needs to look at the residual plots, which refer to the distance between the reconstructed track intersect and the pixel in which a hit was detected within one detector plane (local). These plots were created by applying a Gaussian fit to the residual histograms present for each telescope plane in the Tracking4D root-directory and plotting their mean values with standard deviation as the error bars.

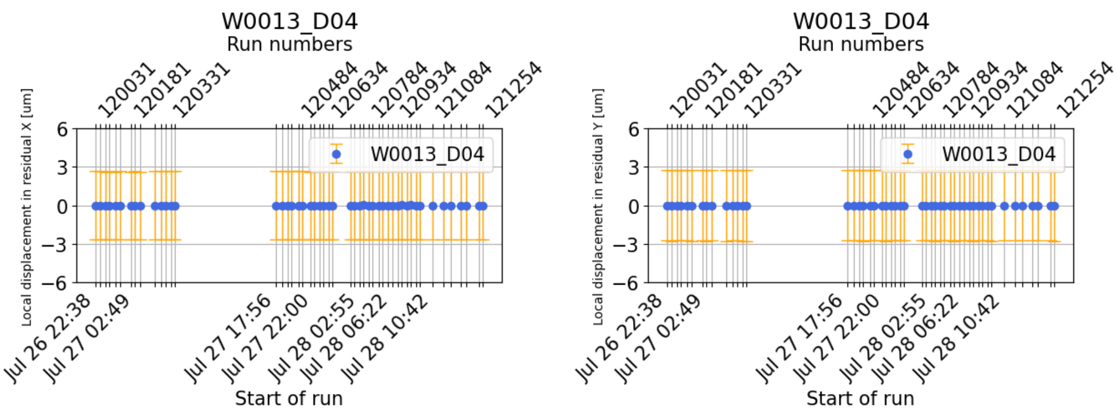


Figure 6: Means (blue dots) and standard deviations (yellow errorbars) of the residual distances for the first upstream plane W0013_D04. in x (left) and y (right). For plots relating to the other planes see Appendix B of Section 6

As seen in the plots the extracted mean residual are all centered around zero. This shows that the detector planes are all well aligned, and that the plots of displacement are valid. If the alignments were incorrect, the residual plots would be centered around values different from 0, and for really poor alignments, the means would be about one pixel pitch or more.

### 3.2.2 Alignment stability

With the residual plots cofirming the validity of the alignment, the following plots could be produced utilizing a custom made python script. Processing the temperature data acquired through the use of the previously mentioned BME280 detector[7] and the alignment/displacement data gathered through the help of the Corryvreckan reconstruction framework.

The first two plots illustrate the position shift in x and y compared to the reference plane (G02). From these there appears to be an inverse correlation between temperature and shift in the positive direction equating to a negative shift of 0.75 µm per increase in °C in x. Although the gap in displacement data does make it difficult to see how/if the shifts follow the temperature curve. Similar observations apply to the y axis. The z position is set by the telescope operator as a fixed parameter and is therefore not shown, as it does not change.

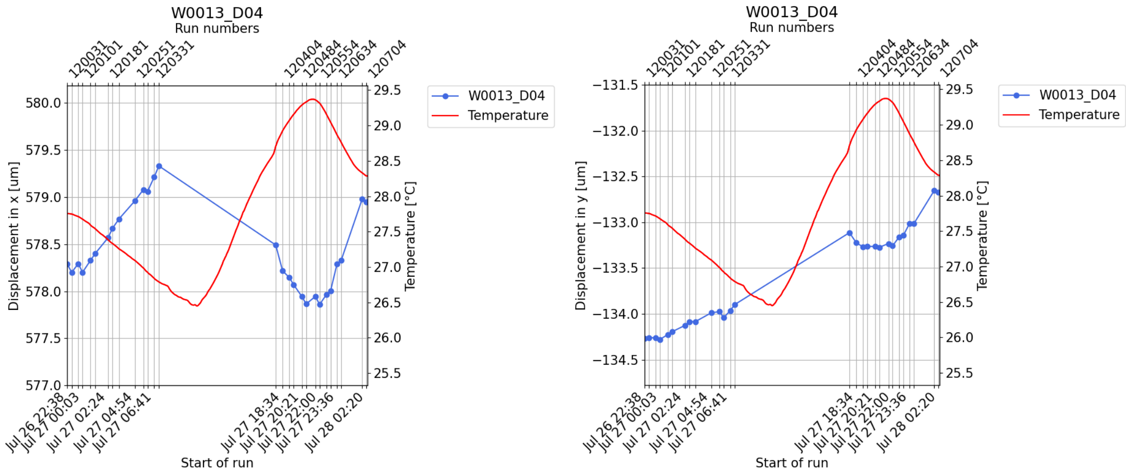


Figure 7: Position-wise shifts for the first upstream plane W0013_D04 in x (left) and y (right) + temperature. For plots relating to the other planes see Appendix B of Section 6

For the angular plots, it would seem that there is an inverse correlation between the shift in x compared to temperature and a regular correlation for shifts in y in relation to temperature. Due to the large gap in available telescope measurement data in the presented time interval only a tendency can be found.

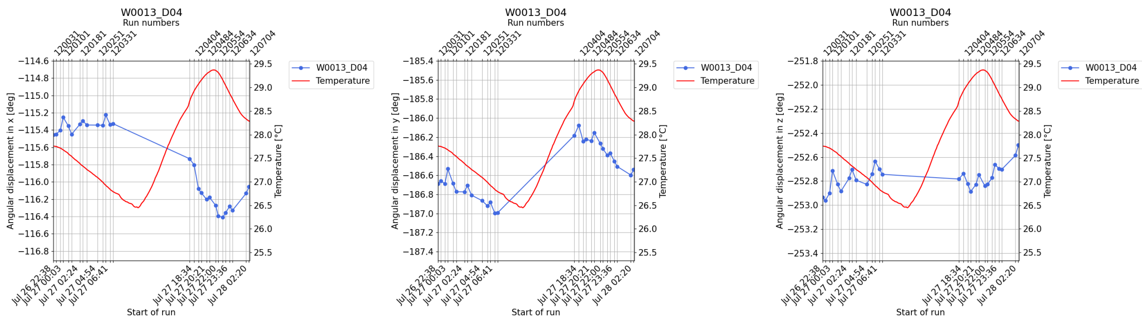


Figure 8: Angular shifts for the first upstream plane W0013_D04 in x (left), y (middle) and z (right). For plots relating to the other planes see Appendix B of Section 6

### 3.2.3 Comparison of different planes

For a comparison of the different planes with each other. The various alignment shifts are plotted together with respect to the initial values of the first run.
For both x and y in the position plots, shifts are clearly visible The biggest change in x seem to occur for the E03 plane, while D04 has largest fluctuations. D04 has the largest shift followed closely by G03, and although the fluctuations of J05 and L09 in y aren't as large as they were for D04 in x, they are still visible.

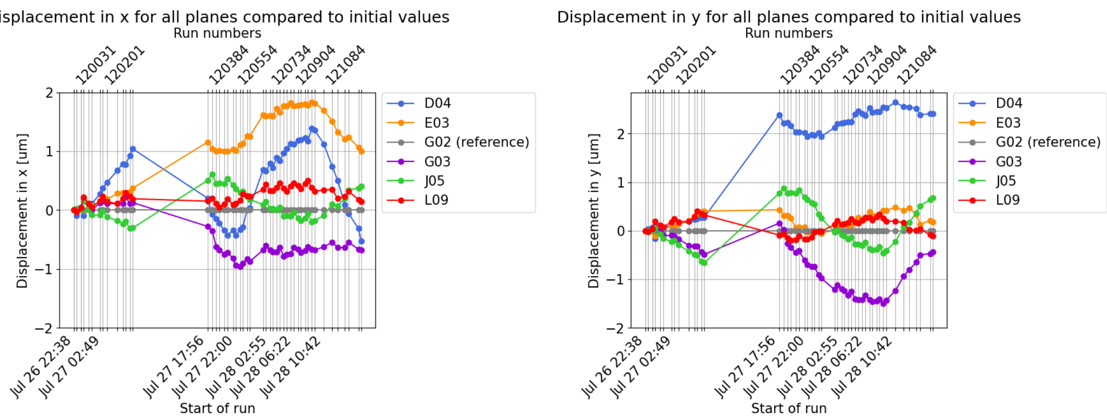


Figure 9: Plots of the position-wise shifts for all planes compared to their initial values in x (left) and y (right)

For the angular plots, a saw-tooth-like pattern can be seen, however, the shifts are very small, mostly within 0.1 degree, which is below the angular alignment precision of the telescope.

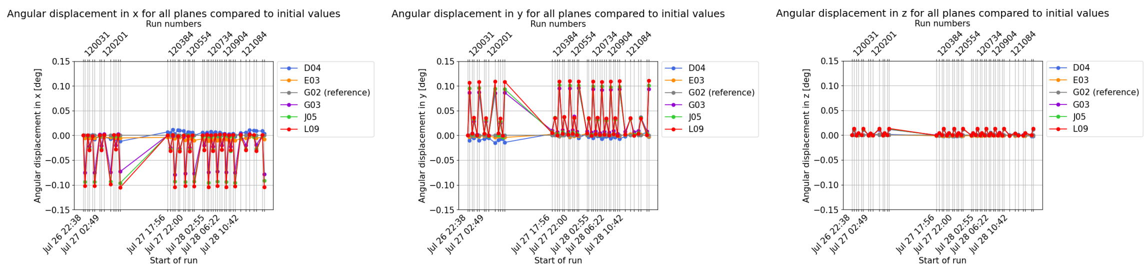


Figure 10: Plots of the angular shifts for all planes compared to their initial values in x (left), y (middle), z (right)

Although it must be restated that all of positions are with respect to the reference plane, so the shifts of the planes are coupled to the shifts of that one plane.

## 3.3 Air cooling and circulation station

As an addition to the telescope setup a compressor cart was previously designed and constructed by the team.

Figure 11: Compressor cart from left to right a) front, b) right side, c) back, d) left side

The purpose of adding a low-volume air flow to the supporting services of the telescope is to improve the air-circulation, introducing a consistent and enhanced heat dissipation for DUTs as well as telescope planes. Both are usually encapsulated by plastic covers protecting from stray light and mechanical damage. The air passes through a filter and a membrane dryer stage limiting the buildup of moisture in the system. The distribution among the different detector planes is facilitated using a series of tubes and distribution blocks.

## 3.4 Sensors

With the compressor added to the telescope setup, sensors monitoring the temperature, humidity, pressure and flow of the air become a necessary addition to ensure the stability of the system. As part of this project three detectors were set up to monitor temperature and humidity as well as total and differential pressure of the air flowing through the telescope, and the data collected could be visualized via the visualization web application Grafana.

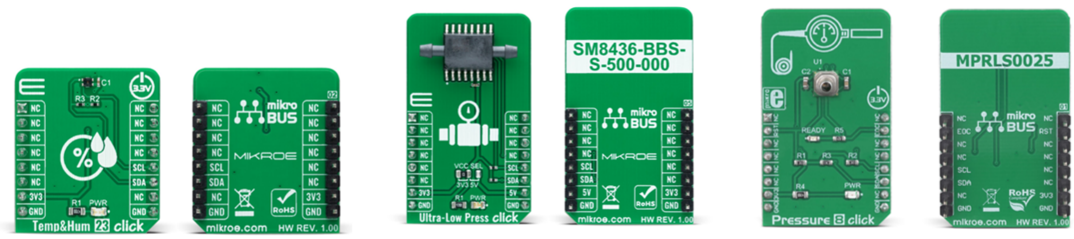


Figure 12: From left to right a) MIKROE Temp&Hum 23 Click, b) MIKROE Ultra-Low Press Click c) MIKROE Pressure 8 click

Two BME280 sensor[7] had also been added previously, with one being mounted on the cart, and the other placed within the telescope itself. Here they measure ambient temperature, relative humidity and pressure. Data gathered from these sensors were only accessed for comparison and to act as baseline measurements of pressure, humidity and temperature.

### 3.4.1 Temperature & humidity sensor (MIKROE Temp&Hum 23 Click)

To monitor the temperature and humidity of the air flowing through the telescope, the MIKROE Temp&Hum 23 Click was chosen due to its relatively low cost and ultra-low-power relative humidity and temperature sensor, the SHT45 by Sensirion[8]. This particular sensor is capable of detecting relative humidity between 0% and 100% and temperatures ranging from -40°C to 125°C with accuracy within 1% for the humidity and 0.1°C for the temperature
The detector was read out using a CM4 Nano[9], a third party embedded computer based on a Raspbbery Pi CM4[10], which itself is a type of small single-board computers widely used due to their small size, low cost, modularity and open design. The connections to the sensors were established using a MIKROE UNI Clicker and Shuttle Click[11]. The Raspberry Pi is able to receive recorded data and process it using a python script based on the adafruit_sht4x library package[12]. In this configuration the sensor provides the readings seen in Figure 13

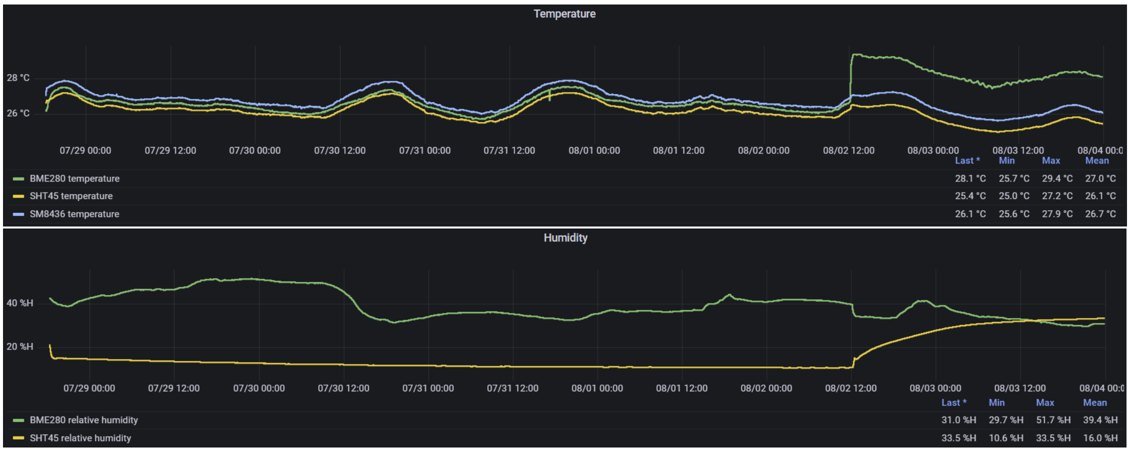


Figure 13: Grafana graphical user interface plotting the measured temperature (upper) and humidity (lower) by the MIKROE Temp&Hum 23 Click compared to readings provided by the BME280 ambient sensor

### 3.4.2 Pressure sensor (MIKROE Pressure 8 click)

In order to measure the total pressure of the air within low-pressure tank of the compressor cart, the MIKROE Pressure 8 click was chosen.
The detector is implemented in the same way as the MIKROE Temp&Hum 23 Click, but with the use of a python script based on the adafruit_mprls library package[13]. Due to the fact that the MPRLS0025PA00001A[14], which was the sensor-module that the MIKROE board originally was fitted with, had a maximal range of 0 to 1724 hPa in absolute pressure (what the PA stands for in product code), it was exchanged for another sensor module. The module chosen was the MPRLS0030PG00000A[14]. This sensor had a range of 0 to 2068 hPa in gauge pressure (PG), meaning pressure above atmospheric pressure. However, the readout of the two sensor modules were still compatible due to having the same type of transfer function (both module names ending in A), despite having differing $I^2C$ addresses (signified by the second to last index module name). Another issue did arise although, as

during the process of soldering and fixing the new sensor module to the board, the inlet for reference ambient pressure readings was blocked. Thereby the sensor stopped being able to read pressure accurately, and after a few days started to malfunction which eventually led to a complete shut down. The initial pressure reading was accurate, and fits the approximate 2 bar above ambient pressure inside the pressure tank of the compressor setup. This can be seen in Figure 14


Figure 14: Grafana graphical user interface plotting total pressure measured by the MIKROE Pressure 8 click

### 3.4.3 Differential pressure sensor (MIKROE Ultra-Low Press Click)

The third sensor incorporated into the setup as part of this project was the MIKROE Ultra-Low Press Click. It was chosen due to its high precision and range going from 0 to 250 Pa differential pressure.

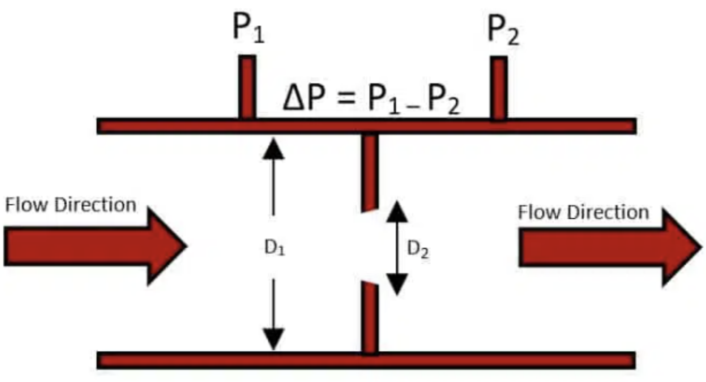


Figure 15: Illustration of what how differential pressure is measured [15]

Once again a MIKROE UNI Clicker and Shuttle Click[11] connected to a Raspberry Pi was used for device interconnection and communication. Since there was no available library/package to base a script on, a custom package had to be written. With the adafruit_sht4x package as the template, and by reworking it based on the information provided in the SM8436 product data sheet[16], a new custom package was created. The main difference between the sht4x and the new custom package was how the data is read from the

sensors. The sht4x sensor is using 6 bytes, the first two holding the temperature readings, while the fourth and fifth byte would hold the humidity data. The third and the sixth transport the respective crc (cyclic redundancy check) values, which are generated alongside the actual readings to provide an additional check on the transferred values. However the crc won't hinder the transfer of data that is wrong or corrupted. The sm8436 is using 9 bytes for data transfer, and through testing, the byte layout and storage was investigated, and the internal temperature as well as the differential pressure measured by the sensor could be read out. The working package was published for others to use on Pypi under the name of sensor-sm8436-package 0.0.1.[17]
And with this new package it became possible to receive differential pressure readings,$p_{diff}$, along for calculation of the airflow, $f_{air}$ which was obtained using Equation 1

$$f_{air} = v_{air} \cdot A_{pipe} \quad \text{with} \quad v_{air} = \sqrt{2\frac{p_{diff}}{\rho_{air}}} \quad \text{and} \quad A_{pipe} = \pi \cdot r^2 \tag{1}$$

$$\rho_{air} = \frac{p}{R_{air} \cdot T} \quad \text{where} \quad R_{air} = 287.05\frac{\text{J}}{\text{kg} \cdot \text{K}} \tag{2}$$

By inserting the value of the specific gas constant for air, $R_{air}$, and the Calculated area the air restrictor, $A$ with a radius of $r = 1.5$ mm into Equation 1 along with a pressure, $p$, of 2000 hPa, which was the initial measurement from the Ultra-Low Press Click before it malfunctioned, and the temperature reading, $T$, one gets the final equation, used for calculating the airflow3

$$f_{air} = 7 \cdot 10^{-6}\text{m}^2 \cdot \sqrt{\frac{p_{diff}}{348.37\frac{\text{kg}}{\text{m}^3 \cdot \text{K}} \cdot T}} \tag{3}$$

The fixed pressure value used also explains why the flow doesn't go to zero, as the compressor was switched off, as seen in Figure 3.4.3

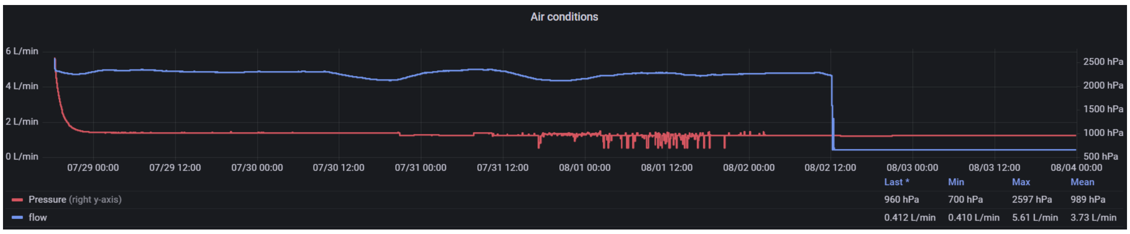


Figure 16: Grafana graphical user interface plotting the differential pressure measured by the MIKROE Ultra-Low Press Click and the calculated airflow

# 4 Outlook & Conclusion

Throughout this summer student project several improvements have been made to the telescope setup. However, there still remains ample opportunity for improvement. The first is to repair or replace the faulty pressure sensor. Another way to further the understanding of the shifts of the telescope planes would be to collect these observables over a longer time frame. In this project, the 49 runs being tracked and analyzed all occurred within the span of two days. Including more runs over a longer time period could improve the statistics of the data and maybe even show recognizable patterns when compared to shifts in temperature.

In conclusion this project has shown that through the optimization of the telescope's mechanical alignment as well as the inclusion of monitoring, in particular of temperature, changes in alignment of the Timepix3 detector planes seem to follow the changes in temperature leading to changes of within 2 µm in translation and 0.1 degree in rotation. And although these changes in alignment might seem small, the feature sizes of the Timepix3 detector assemblies are 55 µm and for some the DUTs it is even smaller (down to around 10 µm). So a change of a few µm is significant, and it especially becomes a problem, if the shifts start accumulating over multiple runs.
Furthermore, with the addition of the compressor cart and the new sensors, the telescope will now be supplied with a known dry airflow making sure that telescope planes are in the best condition for data acquisition, And the improved monitoring will in general help create an even more stable measurement environment for future tests beam campaigns.

# References

[1] The Medipix Collaborations. Timepix3. Technical report, CERN.

[2] Robbert Geertsema. Dialing back time on timepix3: A study on the timing performance of timepix3. 2019.

[3] B. van der Heijden et al. Spidr, a general-purpose readout system for pixel asics. *IOPP's Electronics Journal*, 2017.

[4] D. Dannheim et al. Detector technologies for clic. Technical report, CERN, 2019.

[5] M. Krammer. Silicon detectors in high energy physics experiments, 2015.

[6] Hamamatsu Photonics K.K. Microchannel plate-photomultiplier tubes (mcp-pmt) r3809u series. Technical report, Hamamatsu Photonics K.K., 2023.

[7] Bosch. Bme280 – data sheet. Technical report, Bosch, 2018.

[8] Sensirion. Sht4x. Technical report, Sensirion, 2022.

[9] EDA TEC. Cm4 nano: Raspberry pi cm4 powered industial computer. Technical report, EDA TEC, 2021.

[10] Raspberry Pi Ltd. Raspberry pi compute module 4. Technical report, Raspberry Pi Ltd, 2023.

[11] MikroElektronika (MIKROE). *Uni Clicker User Manual*, 2020.

[12] ladyada. Python library for sensirion sht4x temperature and humidity sensors, 2021 - 2023. https://docs.circuitpython.org/projects/sht4x/en/latest/.

[13] ladyada. Circuitpython library to support honeywell mprls digital pressure sensors., 2021 - 2023. https://docs.circuitpython.org/projects/mprls/en/latest//.

[14] Honeywell Advanced Sensing Technologies. Mpr series. Technical report, Honeywell International Inc, 2022.

[15] E.S. Systems. How to calculate gas flow rate from a pressure measurement?, 2018.

[16] TE Connectivity Corporation. Smi ultra-low pressure digital sensor sm8436 series gage pressure sensors. Technical report, TE Connectivity, 2020.

[17] M. Thøgersen. Sensor_sm8436_package.

# 5 Appendix A

| | Timepix | Timepix3 | Timepix4 |
|---|---|---|---|
| Tech. node (nm) | 250 | 130 | 65 |
| Year | 2005 | 2014 | 2019 |
| Pixel size (mm) | 55 | | |
| # of pixels | 256 x 256 | | 448 x 512 |
| Time bin (resolution) | 10 ns | 1.5 ns | 200 ps |
| Readout architecture | Frame based (sequential R/W) | Data driven or Frame based (sequential R/W) | Data driven or Frame based (sequential or continuous R/W) |
| Number of tilling sides | 3 | | 4 |

Figure 17: Table listing the differences between Timepix, Timepix3 and Timepix4

# 6 Appendix B

## 6.1 W0013_E03

### 6.1.1 Residual plots

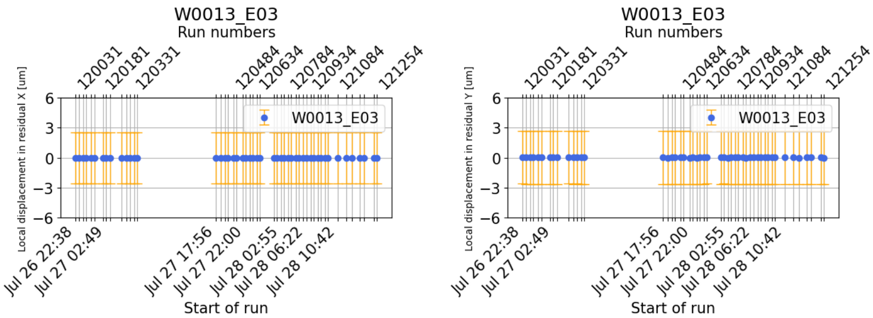


Figure 18: Plots of the residual values with uncertainty for E03 in x (left) and y (right)

### 6.1.2 Individual plots

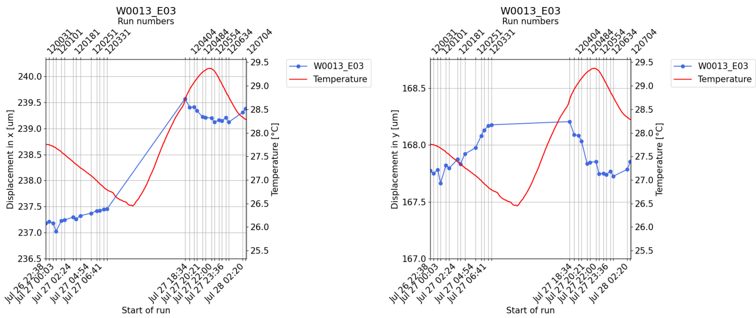


Figure 19: Plots of the position change of E03 in x (left) and y (right)

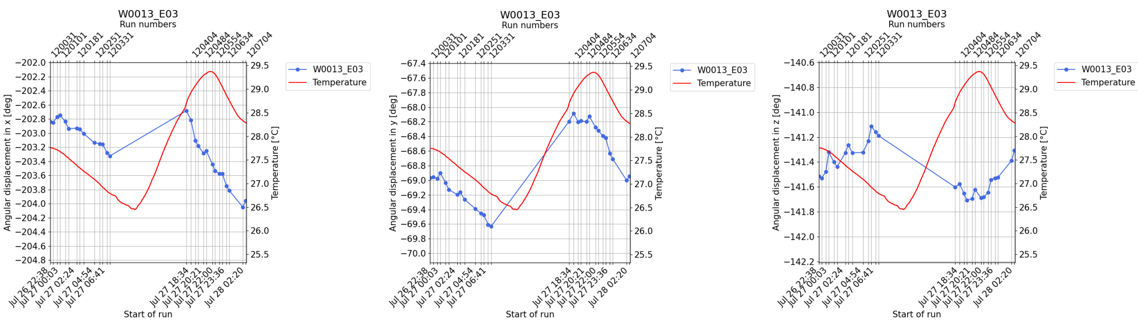


Figure 20: Plots of the angular change of E03 in x (left), y (middle) and z (right)

## 6.2 W0013_G02 (Reference plane)

### 6.2.1 Residual plots

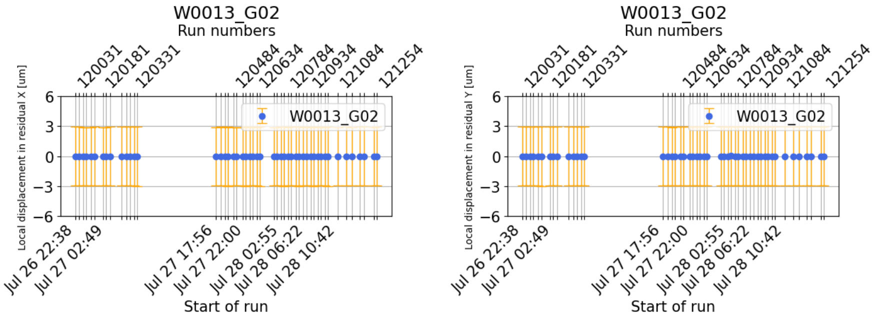


Figure 21: Plots of the residual values with uncertainty for G02 in x (left) and y (right)

### 6.2.2 Individual plots

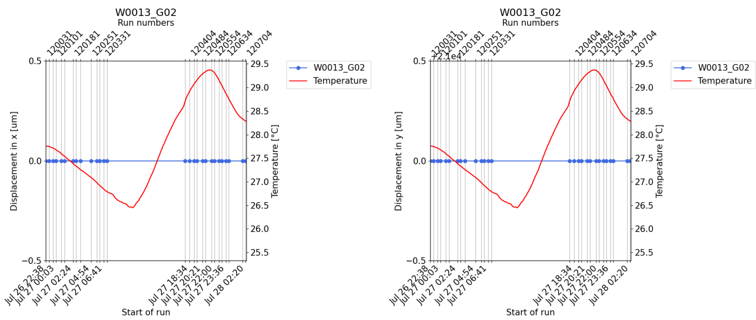


Figure 22: Plots of the position change of G02 in x (left) and y (right)

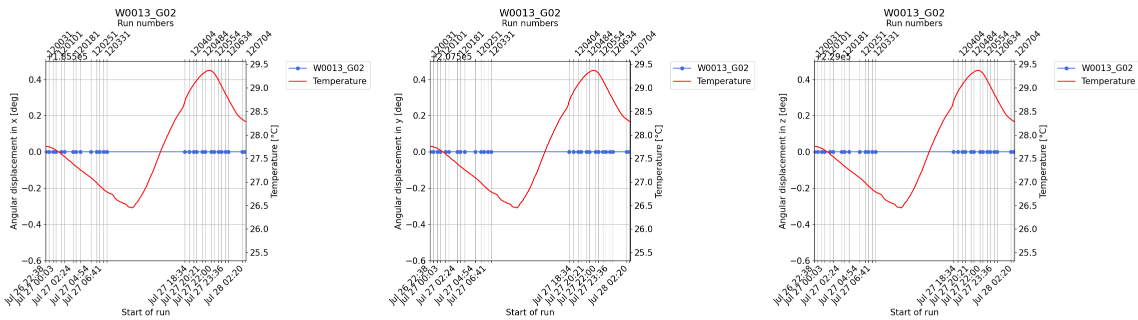


Figure 23: Plots of the angular change of G02 in x (left), y (middle) and z (right)

## 6.3 W0013_G03

### 6.3.1 Residual plots

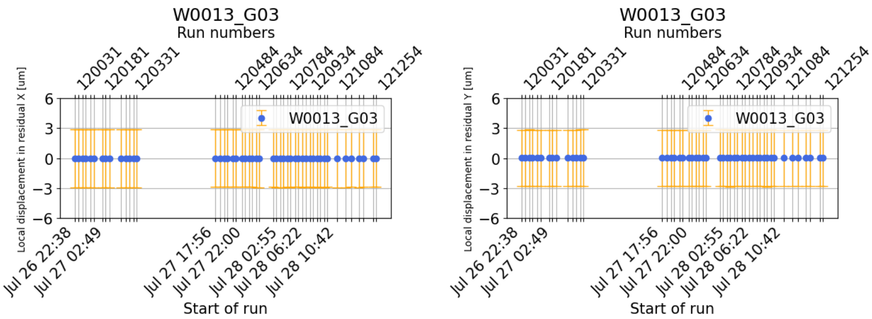


Figure 24: Plots of the residual values with uncertainty for G03 in x (left) and y (right)

### 6.3.2 Individual plots

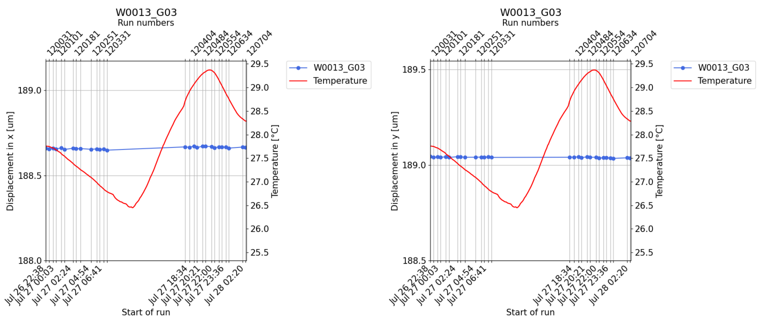


Figure 25: Plots of the position change of G03 in x (left) and y (right)

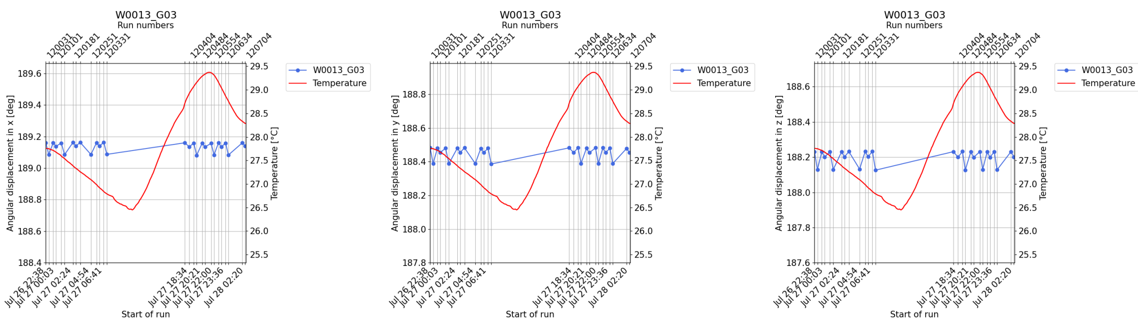


Figure 26: Plots of the angular change of G03 in x (left), y (middle) and z (right)

## 6.4 W0013_J05

### 6.4.1 Residual plots

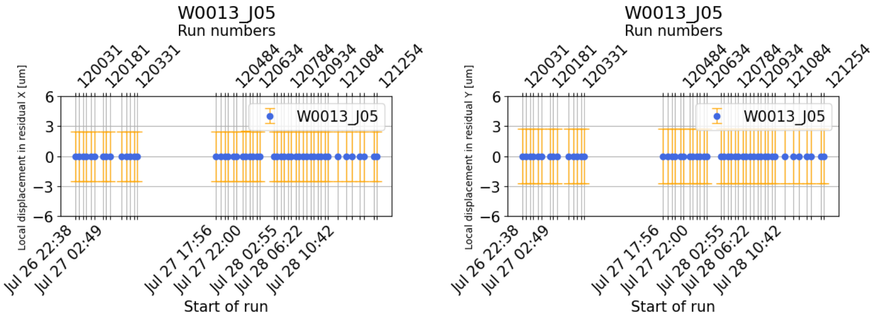


Figure 27: Plots of the residual values with uncertainty for J05 in x (left) and y (right)

### 6.4.2 Individual plots

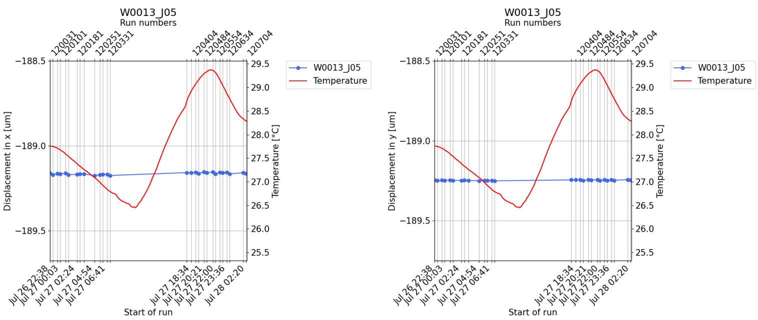


Figure 28: Plots of the position change of J05 in x (left) and y (right)

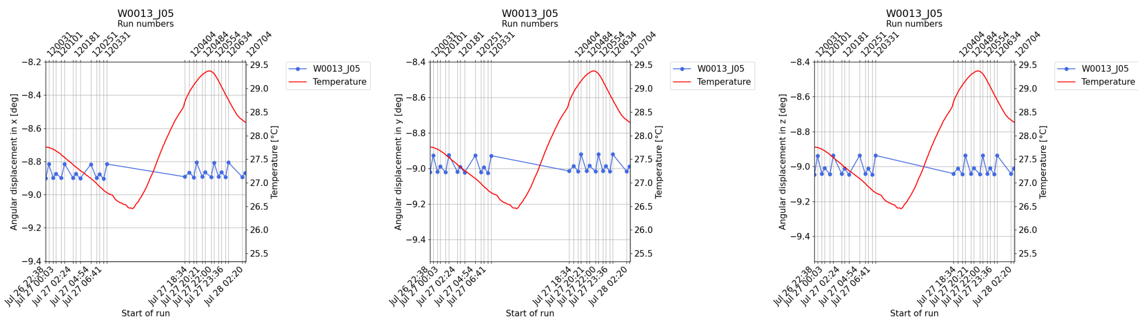


Figure 29: Plots of the angular change of J05 in x (left), y (middle) and z (right)

## 6.5 W0013_L09

### 6.5.1 Residual plots

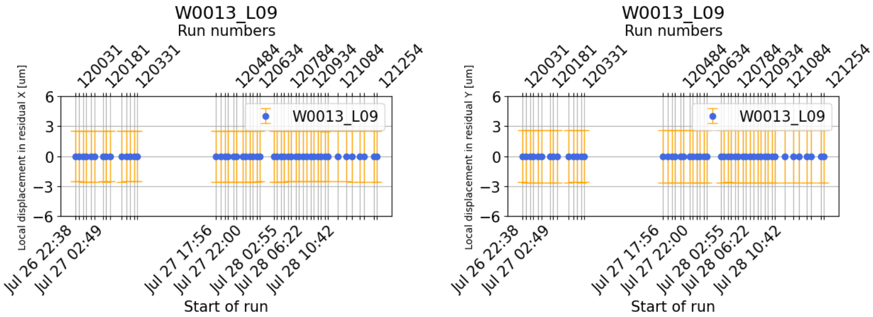


Figure 30: Plots of the residual values with uncertainty for L09 in x (left) and y (right)

### 6.5.2 Individual plots

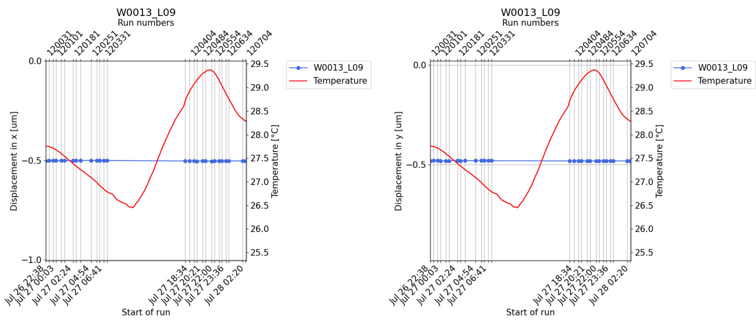


Figure 31: Plots of the position change of L09 in x (left) and y (right)

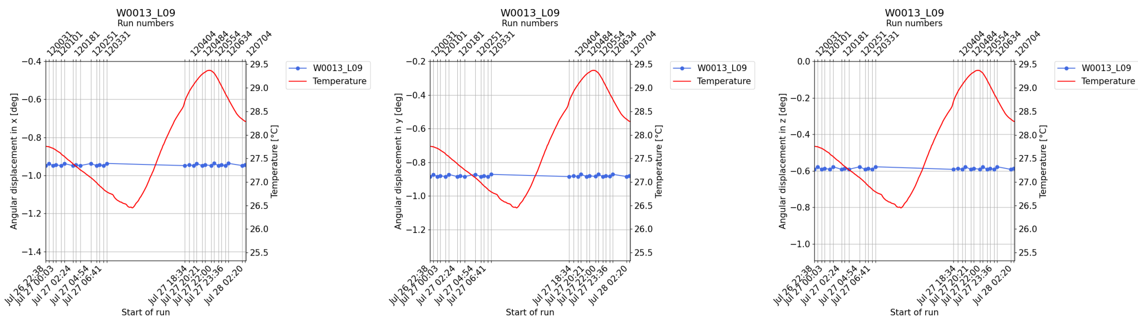


Figure 32: Plots of the angular change of L09 in x (left), y (middle) and z (right)